Chemical Engineering Journal 477 (2023) 147090

Contents lists available at ScienceDirect

Chemical Engineering Journal

journal homepage: www.elsevier.com/locate/cej

Highly transparent, durable, and omniphobic liquid-like coatings for efficient dynamic de-wetting and self-cleaning applications

Jianwen Peng [a,b,c], Peng Ye [a,b,c], Fei Xu [a,b,c], Haolei Geng [a,b,c], Ruitao Wang [d], Yuanxu Jiang [a,b,c], Yanji Zhu [e], Huaiyuan Wang [a,b,c,*]

[a] School of Chemical Engineering and Technology and State Key Laboratory of Chemical Engineering, Tianjin University, Tianjin 300350, PR China
[b] Collaborative Innovation Centre of Chemical Science and Engineering (Tianjin), Tianjin University, Tianjin 300072, PR China
[c] Tianjin Key Laboratory of Chemical process safety and equipment technology, Tianjin 300072, PR China
[d] Zhejiang Institute of Tianjin University, Ningbo 315201, Zhejiang, PR China
[e] Tianjin Key Lab Composite & Functional Materials, School of Materials Science and Engineering, Tianjin University, Tianjin 300072, PR China

ARTICLE INFO

Keywords:
Omniphobic
Liquid-like coating
Solar cell
Self-cleaning
Dynamic de-wetting
Transparent

ABSTRACT

Solar cells, which are contributing significantly to achieving carbon neutrality but suffer from the dust deposition problem that limits their power conversion efficiency. Despite the many desirable properties of self-cleaning coatings to improve the efficiency of solar cells, one formidable challenge in designing coatings for their practical applications lies in integrating transparency, durability, and self-cleaning properties. Herein, we report a multifunctional, durable, and omniphobic liquid-like FEVE-g-PDMS coating, which was readily prepared by embedding highly flexible polydimethylsiloxane (PDMS) chains as dynamic de-wetting agent into the fluorinated ethylene-(hydroxyl-alkyl) vinyl ether (FEVE) matrix. The resultant coating exhibited low roughness and high transparency (89.72 % at 550 nm, the air was used as reference), which could be applied to the protective solar cover glass by facile spraying technique. The PDMS chains with high mobility were enriched on the coating surface and could dynamically rotate/bend/stretch to reduce the energy barriers for the moving liquids, endowing coating with unprecedented dynamic de-wetting property. Importantly, the coating demonstrated self-cleaning property, which could readily slide the liquid and dust contaminants off, resulting in a high efficiency recovery ratio for solar cells (95.37 %). Besides, the coating showed strong adhesion, and durability to ultraviolet rays, humidity and thermal atmospheres, and chemical media. Therefore, the synthetic omniphobic liquid-like coating holds great promise for the development of innovative self-cleaning materials with versatility and durability that are not realizable with conventional solid interface engineering.

1. Introduction

In response to the growing global greenhouse effect and the imperative to achieve carbon neutrality, the reduction of carbon emissions and the development of renewable energy are crucial [1]. It is generally accepted that renewable energy sources (i.e., solar, wind, and hydro, etc.) can provide more than 3,000 times the current global energy demand [2]. Among them, solar energy is an inexhaustible resource, which has the advantages of renewable, clean, and ubiquitous properties [3]. Solar cells, also known as photovoltaic (PV) cells, are recognized as a powerful strategy to utilize solar energy and have been industrialized on a large scale [4,5]. The cover glass provides mechanical rigidity and thermal stability for solar cells in harsh environments, but contaminants such as dust, organic waste, and water droplets inevitably reduce the efficiency of solar cells [6,7]. Specifically, lots of outdoor soiling tests have confirmed that the performance of PV modules decreased by 78 % after one year of outdoor exposure without any cleaning [8,9].

To cope with the dust deposition on PV modules, the cover glass must be cleaned regularly. Up to now, several cleaning methods have been developed, such as natural cleaning [10], manual cleaning [11,12], mechanical and electromechanical cleaning systems [13,14]. However, these methods are either uncontrollable and inefficient or cumbersome and uneconomical, which have become obstacles to their practical application [15–17]. In contrast, self-cleaning surface/coating methods

* Corresponding author at: School of Chemical Engineering and Technology and State Key Laboratory of Chemical Engineering, Tianjin University, Tianjin 300350, PR China.
E-mail address: huaiyuanwang@tju.edu.cn (H. Wang).

https://doi.org/10.1016/j.cej.2023.147090
Received 11 September 2023; Received in revised form 22 October 2023; Accepted 31 October 2023
Available online 4 November 2023

provide an affordable, efficient, and versatile strategy for mitigating dust deposition without the need for labor and complex auxiliary devices [18–20]. Specifically, such methods depend on the superhydrophobicity and superhydrophilicity of the surfaces/coatings, which ensures that they could be readily cleaned by natural water (rainfall). For example, Richards et al. reported a superhydrophobic hot-embossed fluoropolymer film, and the self-cleaning property of the film was verified by cleaning sea sand with water droplets and showing a 93.6 % recovery rate (in terms of short-circuit current density) [21]. Additionally, Zhong et al. fabricated a superhydrophilic self-cleaning coating composed of 3-triethoxysilylpropylamine and TiO_2, which can increase the output of solar cells by 4.3 % [19]. However, super-wettability and transmittance are generally reciprocally exclusive properties for superhydrophobic or superhydrophilic coatings—enhancing one performance usually results in weakened performance in another [5,22,23]. This is because increasing roughness to enhance hydrophilicity or hydrophobicity could also cause light scattering and thus reduce the transmittance of the self-cleaning coating. Furthermore, these coatings with elaborate micro-/nano-structures may lose their self-cleaning properties due to the erosion effects of dust particles, oily waste, and ultraviolet (UV) light outside [5,20,24–26]. Therefore, it is highly desirable to develop a new self-cleaning coating for solar cells that is not reliant on elaborate micro-/nano-structures, and incorporates transparency, omniphobicity, self-cleaning, and durability.

Omniphobic liquid-like coatings with low-surface-energy and dynamic de-wetting properties have been reported as potentially feasible surfaces for practical applications, overcoming the drawbacks of conventional super-hydrophobic/hydrophilic or slippery liquid-infused porous surfaces [27–31]. Specifically, the unique property of omniphobic liquid-like coating is derived from the flexible polymer (such as perfluorinated polyether and PDMS) chains covalently bounded to coating matrix, which are liquid and highly mobile state at room temperature due to the extremely low glass transition temperature (<-100 °C) [27]. Thus, the polymer chains endow the coating with dynamic de-wetting property by converting the solid–liquid interface between the probe droplet and the coating into the liquid–liquid interface with reduced hysteresis [32,33]. Moreover, the omniphobic liquid-like coating is usually smooth and transparent, making it a potential candidate for self-cleaning coating for optical devices. Noteworthily, with regards to the self-cleaning application for the cover glass of solar cells, further requirements are self-cleaning property for deposited dust and prolonged stability for harsh UV conditions. Unfortunately, to the best of our knowledge, there has been little investigation and discussion about the aforesaid properties of the omniphobic liquid-like coating, which greatly restricts their application for solar cells and other optical fields [34].

In this work, monohydroxyl-terminated polydimethylsiloxane (PDMS-OH) was selected as a high mobility polymer to construct the omniphobic liquid-like coating. Owing to the moderate cost and excellent optical property, and the terminal –OH group of PDMS-OH is reactive and can be covalently bonded to the polymer matrix, PDMS is widely used in surface coatings [27,35]. Moreover, the commercial fluorinated ethylene-(hydroxyl-alkyl) vinyl ether (FEVE) was adopted as a matrix for its low-surface-energy, excellent chemical inertness, and weatherability in response to the challenges of rigorous outdoor conditions [21,36]. Additionally, according to the covalent attachment between the –NCO group of hexamethylene diisocyanate trimer (HDIT) and the –OH group of PDMS-OH, the HDIT-PDMS precursor was successfully synthesized, which was the key to eliminating the macro-phase separation of PDMS chains in the coating. The HDIT-PDMS precursor and unreacted HDIT were simultaneously employed as cross-linking agents to further embed the PDMS chains into the matrix, and the highly transparent, durable, omniphobic liquid-like FEVE-g-PDMS coating was thereby prepared. The transmittance of the prepared coating with air as reference was up to 89.72 % (at 550 nm). The unbound and abundant repeating (-O-Si-O-) groups in PDMS chains were highly flexible and thus could be enriched on the coating surface and rotated/bent to exhibit liquid-like properties, endowing the FEVE-g-PDMS coating with omniphobic (WCA = 104.8 ± 0.6°, WSA = 23.8 ± 2.1°, and OSA < 15°) and self-cleaning properties. Meanwhile, the coating showed unprecedented and comprehensive stability, especially UV-resistance, humidity resistance and thermal stability, and chemical durability, which are indispensable for the protective coating of solar cells. More importantly, the coating applied on the cover glass of the solar cell could efficiently clean the deposited dust with the assistance of simulated rainfall during the self-cleaning process and demonstrated a recovery ratio of 95.37 % (in terms of short-circuit current density), which opens up a new field of application for weather-resistant omniphobic coatings. We envision that the FEVE-g-PDMS coating in this work can provide design guidelines for reliable self-cleaning coating in solar cells and other optical device.

2. Experimental

2.1. Materials

Please refer to Text S1 in Supporting Material for details.

2.2. Fabrication of FEVE-g-PDMS coating

In this work, the weight content of PDMS-OH was set as 0, 0.5, 1.0, 1.5, and 2.0 wt% concerning the total solid weights of FEVE and HDIT, and the corresponding cured coatings were named FEVE, FEVE-g-$PDMS_{0.5}$, FEVE-g-$PDMS_{1.0}$, FEVE-g-$PDMS_{1.5}$, FEVE-g-$PDMS_{2.0}$ coating, respectively.

Take the preparation of FEVE-g-$PDMS_{1.0}$ coating as an example. Firstly, HDIT (3.0 g), PDMS-OH (0.22 g), and DBTDL (0.01 g) were mixed with PGMEA (3.0 g), and the resultant mixture was mechanically stirred at 80 °C for 1 h to obtain the precursor solution HDIT-PDMS (Fig. 1a). Thereafter, FEVE (4.0 g) and HDIT-PDMS (0.8 g) were dissolved in BA (8.0 g) and kept magnetically stirred for 15 min to form a coating solution. The resulting coating solution was sprayed on a glass substrate. The FEVE-g-$PDMS_{1.0}$ coating was obtained after curing at 120 °C for 2 h. The schematic illustration for the fabrication of FEVE-g-$PDMS_{1.0}$ coating can be seen in Fig. 1b. The other FEVE-g-PDMS coatings were prepared by the same method, only adjusting the content of PDMS-OH.

2.3. Characterization

The contact angles (CAs) and sliding angles (SAs) of water and oil were measured by a contact angle measuring system (Attention Theta Lite), equipped with a tilting table at room temperature. The volume of liquids used for the CAs measurement was 5 μL, and water and oil volumes for the SAs measurement were 30 μL and 15 μL, respectively. The transmittances of the coatings (the air was used as reference) at five different positions on coated ultra-white float glasses were measured by a UV–visible spectrophotometer (UV–vis, TU-1901), and the visible light average transmittance of the samples (before and after dust deposition, and after self-cleaning progress) was tested by a portable light transmittance meter (Linshang Technology). The chemical structure of the samples was determined by Attenuated Total Reflectance Fourier transform infrared (ATR-FTIR, Perkin Elmer) spectroscopy. The chemical composition of the FEVE-g-$PDMS_{1.0}$ coating surface was analyzed by an X-ray photoelectron spectroscopy (XPS, ThermoFisher Scientific K-Alpha$^+$) with Al Kα X-ray radiation source, and all binding energies were calibrated using the C 1 s peak at 284.8 eV as the reference. The morphological structures and energy dispersive spectrometry (EDS) elemental mapping of coating surface and cross-section were characterized using a scanning electron microscope (SEM, Regulus 8100) equipped with an EDS detector. Topography images and surface roughness of the coatings were obtained by an atomic force microscope

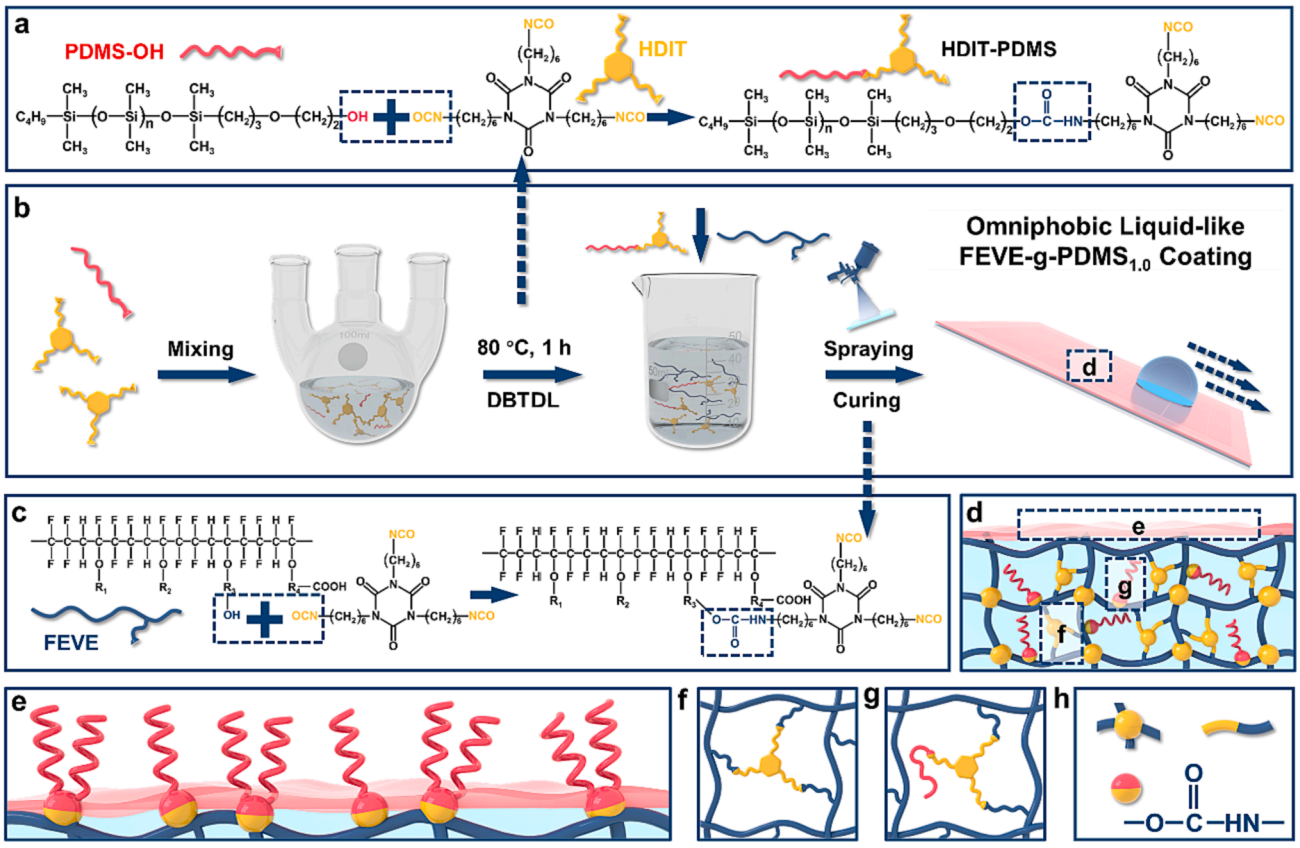

Fig. 1. (a) The synthetic route of HDIT-PDMS. (b) The schematic illustration for the fabrication of FEVE-g-PDMS$_{1.0}$ coating. (c) The chemical reaction between FEVE and HDIT. (d) The schematic illustration of the cross-linking network of the coating. (e) The schematic illustration of the enriched PDMS liquid-like layer. (f, g) The schematic illustration of the cross-linking reaction of HDIT, HDIT-PDMS, and FEVE, respectively. (h) The schematic illustration of –NHCOO- group.

(AFM, Dimension icon, Bruker). The retention force between the coating surface and water droplet (5 μL) was measured using a contact angle measuring system equipped with retention force balance (LSA 100, Lauda Scientific GmbH).

The outdoor natural dust deposition, adhesion strength, wear-resistance, UV-resistance, humidity resistance and thermal stability, and chemical durability tests were described in Text S2-S7.

2.4. Dust deposition simulation apparatus and self-cleaning process

Dust deposition simulation apparatus. In order to obtain a controlled dust deposition process in the laboratory, a dust deposition simulation apparatus was designed. The schematic illustration of the apparatus can be seen in Fig. 5a. The apparatus consists of an acrylic-sealed and transparent test box (30 cm × 30 cm × 20 cm) and an electric powder gun, and the samples are placed in the test box at an angle of approximately 23°. The plateau laterite is chosen as the test dust because it has a similar size and chemical composition to natural dust [37]. The dust deposition density (D, g/m^2) is defined as the ratio of the mass of dust deposited on the sample surface to the sample area, and is calculated by Eq. (1):

$$D = \frac{m_2 - m_1}{S} \tag{1}$$

where m_2 and m_1 are the sample weights after and before dust deposition, respectively. S is the area of the sample.

Self-cleaning process. To quantitatively evaluate the anti-dust and self-cleaning properties of the coatings, a non-touch cleaning system controlled by a micro syringe pump and an electric sliding table was designed and built. The schematic illustration of the system can be seen in Fig. 5b. The micro syringe pump was fixed on electric sliding table, and slid at a velocity of 18 cm/min. The coating sample was placed under the syringe at an angle of about 23°, and the upper edge of the sample was about 5 mm from the syringe tip. The syringe can controllably and quantitatively drop water droplets onto the sample surface to simulate rainfall. Herein, the water droplets were dispensed from the syringe tip at a rate of 3 mL/min. Specifically, for samples with side lengths of 50 mm, the water consumption in a self-cleaning process was about 830 μL, which represents a slight shower [21]. Moreover, the visible light average transmittance of the samples in the dust deposition and self-cleaning process was tested by a portable light transmittance meter, and the schematic illustration of the meter was shown in Fig. 5c.

2.5. Solar cell characteristic test

The simulated solar illumination (AM 1.5 G, 100 mW/cm^2) was provided by a solar simulator (SS150, Zolix) and calibrated with a calibrated Si reference cell. The current density–voltage (J-V) curves of the solar cell covered with different coating samples were measured at four different places using a Keithley 2401 source meter with an active area of 2.00 cm^2 defined by a non-reflective metal shadow mask at a scan speed of 100 mV/s. Moreover, the filling factor (FF) is defined as

$$FF = \frac{I_{MP} \times V_{MP}}{I_{SC} \times V_{OC}} \tag{2}$$

where I_{MP} and V_{MP} are the current and voltage corresponding to maximum output power, respectively; I_{SC} is the short-circuit current at $V = 0$, and V_{OC} is the open-circuit voltage at $I = 0$. Meanwhile, the power conversion efficiency (Eff) is given by Eq. (3):

$$Eff = \frac{J_{SC} \times V_{OC} \times FF}{P_{in}} \times 100 \tag{3}$$

where J_{sc} is short-circuit current density and P_{in} is the power of the solar simulator.

In this work, the self-cleaning capability of the coatings can be compared by the recovery ratio (R, %), defined as the ratio of recovered J_{sc} to the J_{sc} loss due to dust deposition, is calculated by Eq. (4):

$$R = \frac{J_{SC,2} - J_{SC,1}}{J_{SC,0} - J_{SC,1}} \quad (4)$$

where $J_{SC,0}$, $J_{SC,1}$, and $J_{SC,2}$ are the short-circuit current density of the solar cells covered with initial, contaminated, and cleaned glass or coating samples, respectively. The higher the R value, the better self-cleaning capability of the sample.

3. Results and discussion

3.1. Synthesis and characterization of the coatings

A judicious strategy to construct omniphobic liquid-like polymer coating is to embed PDMS chains with low-surface-energy and high mobility into the polymer matrix. Notably, to obtain a highly transparent liquid-like coating, the macro-phase separation of the PDMS chains in the polymer matrix must be eliminated first. Herein, a precursor HDIT-PDMS was synthesis by covalent attachment of PDMS-OH to HDIT, and the schematic illustration of the synthesis process can be seen in Fig. 1a and b, and the chemical structure of PDMS-OH, HDIT, HDIT-PDMS was determined by ATR-FTIR spectrums and shown in Fig. 2a. The characteristic peaks at 1412 cm^{-1} and 1258 cm^{-1} (asymmetric vibration peaks of $-CH_3$ in $Si(CH_3)_2$), 2962 cm^{-1} (asymmetric stretching vibration $-CH_3$), 1080 cm^{-1} (asymmetric expansion vibration peak of the Si-O-Si), and 790 cm^{-1} (vibration absorption peak of Si-CH_3) were observed for PDMS-OH [38–40]. For HDIT and HDIT-PDMS, the absorption in 2262 cm^{-1} and 1683 cm^{-1} can be assigned to the stretching vibrations of –NCO and -C = O group [33,41]. Furthermore, the appearance of a new peak at 803 cm^{-1} (the vibration absorption peak of Si-CH_3 groups of PDMS-OH) in HDIT-PDMS and FEVE-g-PDMS coating and the disappearance of –NCO group at 2262 cm^{-1} corroborated the introduction of PDMS-OH and the consumption of –NCO groups of HDIT-PDMS during the curing process, respectively [42,43]. In addition, identical conclusions were obtained by comparing the ATR-FTIR spectra of FEVE resin, FEVE, and FEVE-g-$PDMS_{1.0}$ coating, and the corresponding spectra and descriptions were provided in Fig. S2 and Text S8.

To further verify the chemical composition of the FEVE-g-$PDMS_{1.0}$ coating, the XPS measurement was performed. As shown in Fig. 2b, the Si 2 s and Si 2p peaks at 152.1 and 101.1 eV were detected, and the Si content of 12.75 % (at an atomic percentage) demonstrated the existence of an abundant PDMS chain on the surface of FEVE-g-$PDMS_{1.0}$ coating. Concretely, the C 1 s and Si 2p high-resolution spectrum can be seen in Fig. 2c and d, the peaks at 291.1, 289.7, 286.3, and 284.8 eV were recognized, corresponding to -CF_2, -C = O, C-N/C-O, and C-C/C-H/C = C of FEVE resin, and the peaks at 103.9 and 102.3 eV can be assigned to Si-O-Si and Si-C-H of PDMS [44–46]. These results confirmed that the plentiful PDMS chains were successfully grafted into the FEVE coating and enriched on the coating surface during the curing process. Moreover, the schematic illustration of the cross-linking network and chemical reaction of the coating can be seen in Fig. 1d–h. Through the reaction of –NCO group in HDIT (HDIT-PDMS) and –OH group in FEVE to form a carbamate bond, a well-crosslinked network was established in the FEVE-g-$PDMS_{1.0}$ coating.

3.2. Transparency, omniphobicity, and surface morphologies of the coatings

High transparency is a prerequisite for self-cleaning applications of

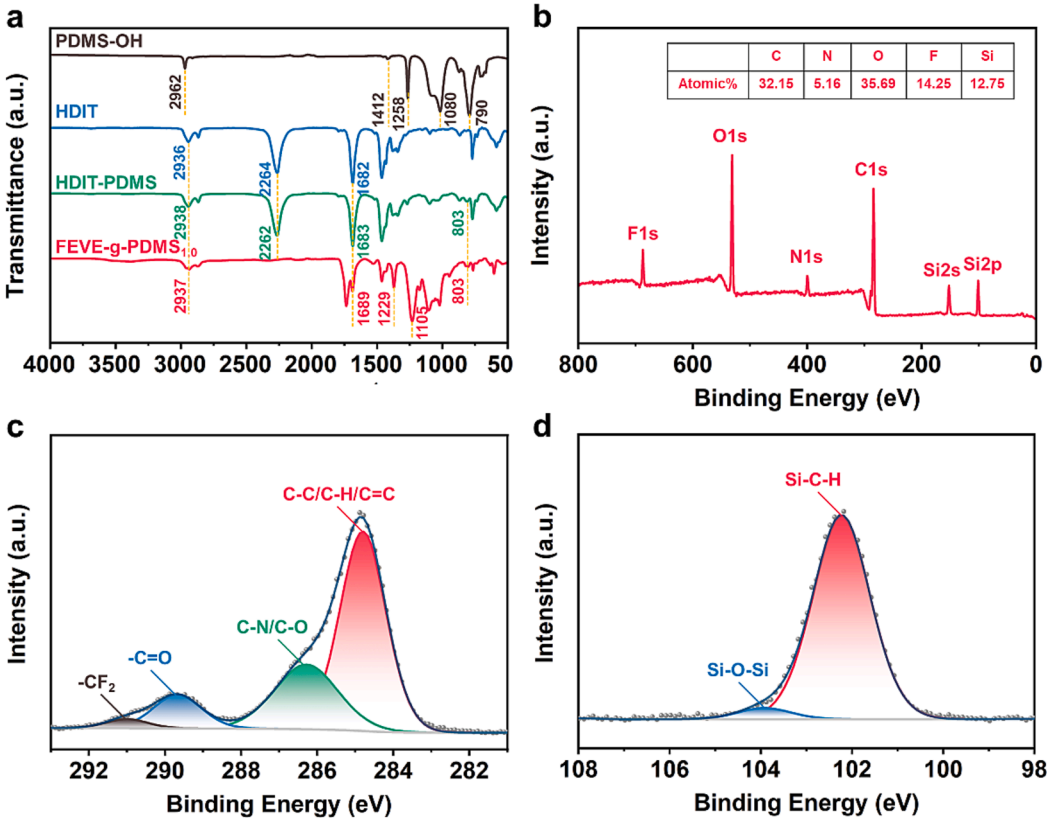

Fig. 2. (a) ATR-FTIR spectra of PDMS-OH, HDIT, HDIT-PDMS, and FEVE-g-$PDMS_{1.0}$ coating. (b) XPS survey spectra, (c) high-resolution C 1 s, and (d) high-resolution Si 2p spectrum of FEVE-g-$PDMS_{1.0}$ coating.

omniphobic liquid-like coatings in the optical devices such as solar cells. The UV–vis transmission spectra of the coatings were shown in Fig. 3a, FEVE coating and all FEVE-g-PDMS coatings displayed high transmittance. Specifically, the transmittance with air as a reference of FEVE, FEVE-g-PDMS$_{1.0}$, and EVEE-g-PDMS$_{2.0}$ coatings at 550 nm were 90.64 %, 89.72 %, and 87.49 %, respectively. It is worth noting that the transmittance of the FEVE-g-PDMS$_{1.0}$ coating was up to 96.93 % when the ultra-white float glass substrate was used as the reference (Fig. S3). Moreover, the FEVE-g-PDMS$_{1.0}$ coating showed excellent optical clarity, and the QR code behind the glass substrate was visible (inset of Fig. 3a). These results indicate that the low PDMS content in the coating has negligible effect on the transmittance, and the coating has potential application in optical devices.

Additionally, the water contact angle (WCA) and water sliding angle (WSA) of the coatings were measured to verify the contribution of low-surface-energy PDMS content to the omniphobicity of the coatings. As can be seen in Fig. 3b, with the increase of PDMS content from 0 % to 0.5 %, the WCA of the coating significantly increased from 91.1 ± 1.0° to 102.6 ± 0.4°, while the WSA sharply decreased from 68.4 ± 5.2° to 29.6 ± 1.8°. Moreover, the omniphobicity of the FEVE-g-PDMS$_{1.0}$ coating was further enhanced, and the WCA and WSA were 104.8 ± 0.6° and 23.8 ± 2.1°, respectively, confirming that the PDMS chains embedded in the coating endowed the coating with excellent omniphobicity. It is worthwhile mentioning that further increasing the PDMS content would not effectively increase the WCA or decrease the WSA of the coating. Correspondingly, the surface energy of the coatings was calculated by using water and diiodomethane as the probe liquids through the Owens, Wendt, Rabel, and Kaelbe (OWRK) method [47,48], and the corresponding description was available in Table S2, S3, and Text S9. The results were shown in Fig. 3c, low content PDMS could decrease the surface energy of the FEVE-g-PDMS coatings to the values that were substantially lower than FEVE coating (30.44 mN/m).

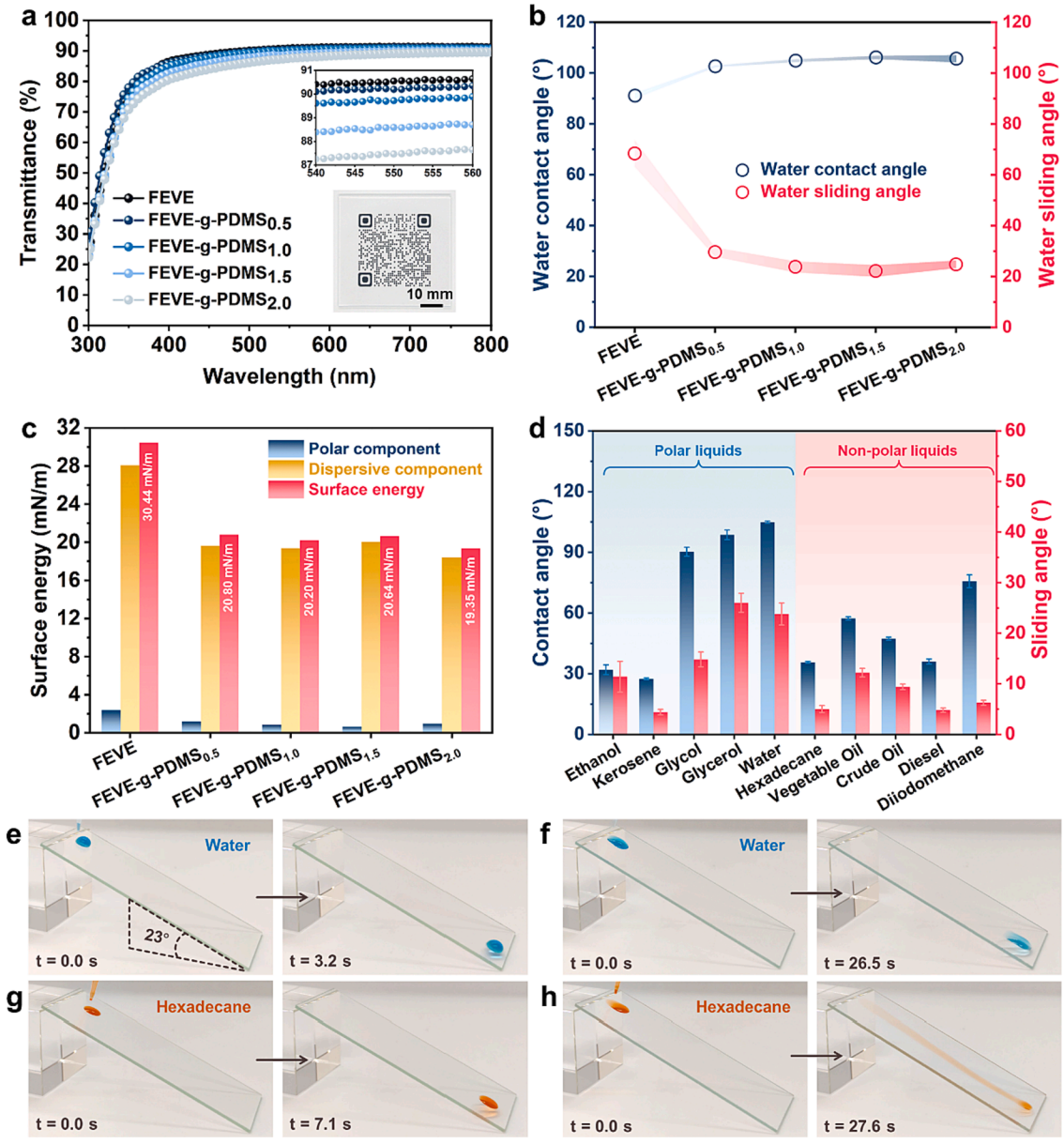

Fig. 3. (a) UV–vis transmission spectra of the coatings. Insets: Photographs of FEVE-g-PDMS$_{1.0}$ coated glass. (b) The water contact angle and water sliding angle of the coatings. (c) The surface energy of the coatings. (d) The contact angle and sliding angle of water and various oil droplets on FEVE-g-PDMS$_{1.0}$ coating. (e-h) Snapshots taken when sliding the water (dyed with methylene blue) and hexadecane (dyed with Sudan IV) on the following samples: FEVE-g-PDMS$_{1.0}$ coating (e, g) and glass (f, h). (For interpretation of the references to colour in this figure legend, the reader is referred to the web version of this article.)

Specifically, the surface energy of FEVE-g-PDMS$_{1.0}$ coating was reduced to 20.20 mN/m with the PDMS content was 1.0 %. Notably, with the increase of PDMS content, the surface energy of the coating tends to be plateaued, which was consistent with the observation from the tendency of the omniphobicity of the coating. Therefore, we selected the FEVE-g-PDMS$_{1.0}$ coating as the optimal sample and for further analyzed it in subsequent studies.

To gain more understanding of the omniphobicity of the FEVE-g-PDMS$_{1.0}$ coating, the dynamic de-wettability of the FEVE-g-PDMS$_{1.0}$ coating was assessed by measuring the CAs and SAs of a wide range of probe liquids, including polar liquids and non-polar liquids. As can be seen in Fig. 3d, with the exception of water and highly viscous glycerol (SAs ≈ 24° and ≈ 26°, respectively), most of the polar and non-polar probe liquids have a SA of below 15° on the coating surface, which confirms the excellent dynamic de-wettability of the FEVE-g-PDMS$_{1.0}$ coating. Furthermore, the dynamic de-wettability of the coating can also be verified by the self-cleaning behavior of the coating. Concretely, Fig. 3e and g showed that the beaded droplets of water and hexadecane spontaneously and swiftly slide off on the tilted FEVE-g-PDMS$_{1.0}$ coating (the tilt angle ≈ 23°) surface without any stain and trace behind. In contrast, both water and hexadecane spread on the bare glass surface, causing noticeable contamination (Fig. 3f and h). These results credibly

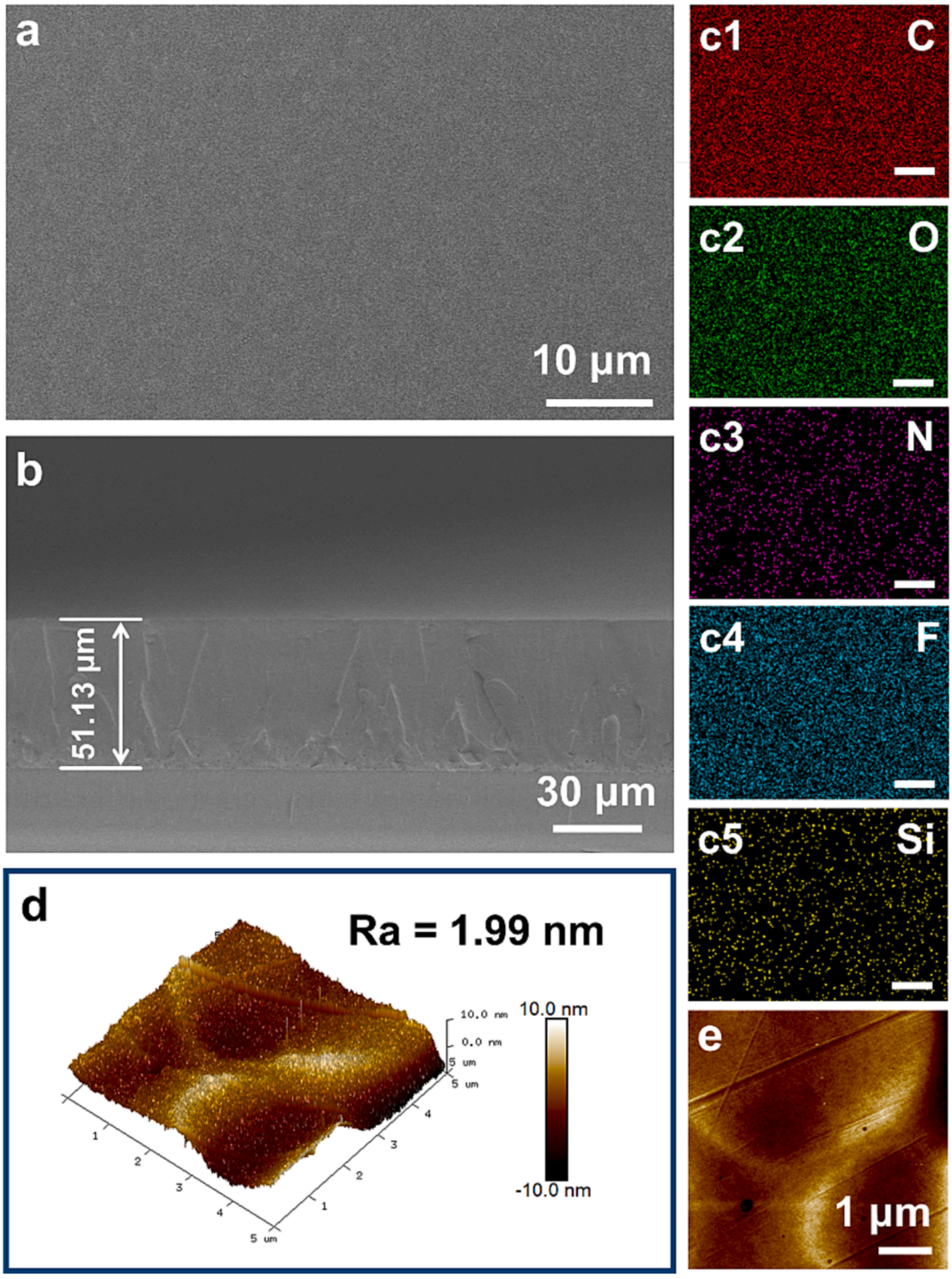

Fig. 4. (a) SEM image of the FEVE-g-PDMS$_{1.0}$ coating surface. (b) Cross-sectional SEM image of FEVE-g-PDMS$_{1.0}$ coating. (c) EDS elemental mapping of the FEVE-g-PDMS$_{1.0}$ coating surface. Scale bar: 10 μm. (d) The three-dimensional and (e) two-dimensional AFM images of FEVE-g-PDMS$_{1.0}$ coating surface.

demonstrate the outstanding dynamic de-wetting property of the omniphobic FEVE-g-PDMS$_{1.0}$ coating, which is essential for self-cleaning applications for solar cells in a variety of harsh conditions.

To further investigate the dynamic de-wettability of the FEVE-g-PDMS$_{1.0}$ coating, the surface morphologies of the coating were investigated in detail by SEM and AFM analysis. As shown in Fig. 4a, the surface morphology of the FEVE-g-PDMS$_{1.0}$ coating was highly smooth and uniform at the micron scale. Moreover, the cross-sectional SEM image displayed that the thickness of the FEVE-g-PDMS$_{1.0}$ coating was about 51 μm and strong adhesion between the coating and the glass substrate can be observed (Fig. 4b). The EDS elemental mapping results of the FEVE-g-PDMS$_{1.0}$ coating surface indicated that the Si element was enriched and homogeneously distributed on the coating surface (Fig. 4c1–c5). Furthermore, AFM analysis was applied to quantitatively investigate the roughness of the coating, and as can be seen in Fig. 4d and e, the FEVE-g-PDMS$_{1.0}$ coating showed extremely low surface roughness (arithmetic mean surface roughness, Ra = 1.99 nm). The enriched PDMS chains on the surface of the FEVE-g-PDMS$_{1.0}$ coating tended to form a liquid-like PDMS layer, which together with the high smoothness endowed the coating with omniphobicity [42,49,50]. In addition, the highly flat and uniform coating surface can reduce the scattering of light, which is also crucial for the transmittance of the coating [51]. In contrast, as shown in Fig. S4, although the FEVE coating also had a relatively low roughness, it did not have PDMS brush layer, and therefore it could not exhibit desired dynamic de-wettability. On the basis of these results, we concluded that the excellent omniphobicity or dynamic de-wettability of the FEVE-g-PDMS$_{1.0}$ coating was derived from the synergy between the enrichment of the low-surface-energy PDMS chains and the extremely low roughness of the coating surface, which suggests their promising self-cleaning applications for solar cells.

3.3. Self-cleaning application of FEVE-g-PDMS$_{1.0}$ coating to solar cells

Contamination caused by dust deposited on the protective solar cover glass severely affects the performance and lifetime of solar cells. For this reason, the feasibility and superiority of the FEVE-g-PDMS$_{1.0}$ coating as a self-cleaning functional surface for solar cells were evaluated by simulating the deposition of dust and the subsequent self-cleaning process. In this work, the simulation apparatus was shown in Fig. 5, where plateau laterite was uniformly sprayed over the FEVE-g-PDMS$_{1.0}$ coating and the dust deposition density (D) was carefully controlled. Moreover, a non-touch cleaning system controlled by a micro syringe pump and an electric sliding table was adopted to quantitatively assess the self-cleaning properties of the coatings (Fig. 5b). As demonstrated in Fig. 5d and e, with the D value increasing from 2 g/m^2 to 24 g/m^2, the visible light average transmittance of the FEVE-g-PDMS$_{1.0}$ coating distinctly decreased from the initial 89.7 % to 27.7 %, which indicated that dust deposition seriously caused transmittance loss of the protective solar cover glass. Remarkably, it can be seen that the FEVE-g-PDMS$_{1.0}$ coating has been heavily covered by dust when D value was up to 24 g/m^2 (Fig. 5d). Surprisingly, there was no significant residual dust on the coating after the self-cleaning process. Additionally, the visible light average transmittance of the FEVE-g-PDMS$_{1.0}$ coating was practically renewed to that before the dust deposition, regardless of the D value (the corresponding optical photographs of the contaminated FEVE-g-PDMS$_{1.0}$ coating were presented in Fig. S5). That is to say, the

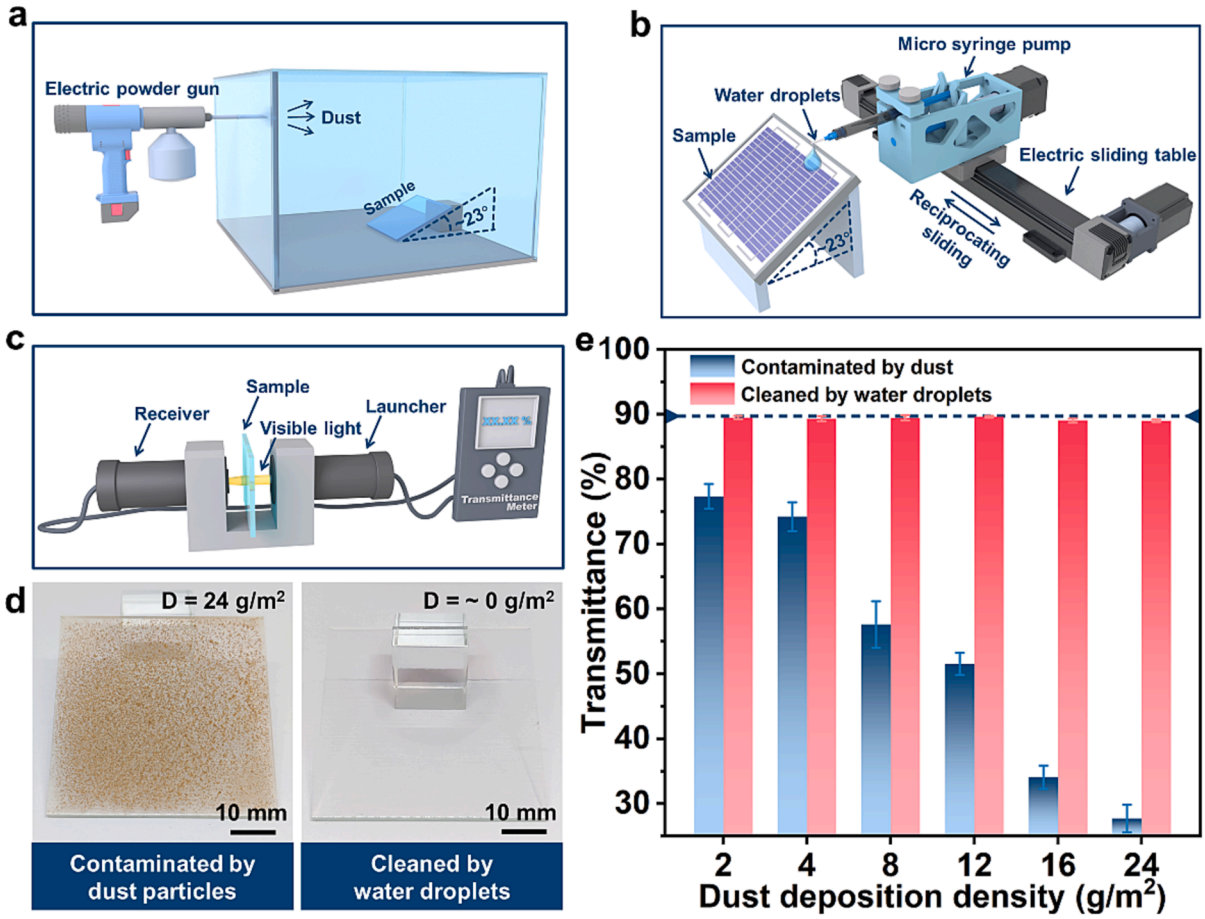

Fig. 5. (a) Schematic illustration of the dust deposition apparatus. (b) Schematic illustration of the self-cleaning system controlled by the micro syringe pump and electric sliding table. (c) Schematic illustration of visible light transmittance meter. (d) Photographs of FEVE-g-PDMS$_{1.0}$ coating contaminated by dust particles and cleaned by water droplets. (e) The visible light average transmittance of contaminated and cleaned coatings at different dust deposition densities.

transmittance of the cleaned coating could reach more than 99 % of the coating before dust deposition. It is important to stress that the volume of water consumed in the self-cleaning process was only equivalent to a slight shower in nature. Furthermore, as shown in Fig. S6, the outdoor dust deposition test (Text S2) was further conducted to verify the self-cleaning property of the coating, and the tested coating still displayed high transparency and good liquid-repellency after 15 d (visible light average transmittance = 87.51 %, WCA = 95.92°, WSA = 50.60°). These results denote that the FEVE-g-PDMS$_{1.0}$ coating with high transparency and efficient self-cleaning property offers exciting opportunities to achieve self-cleaning application for the protective cover glass of solar cells.

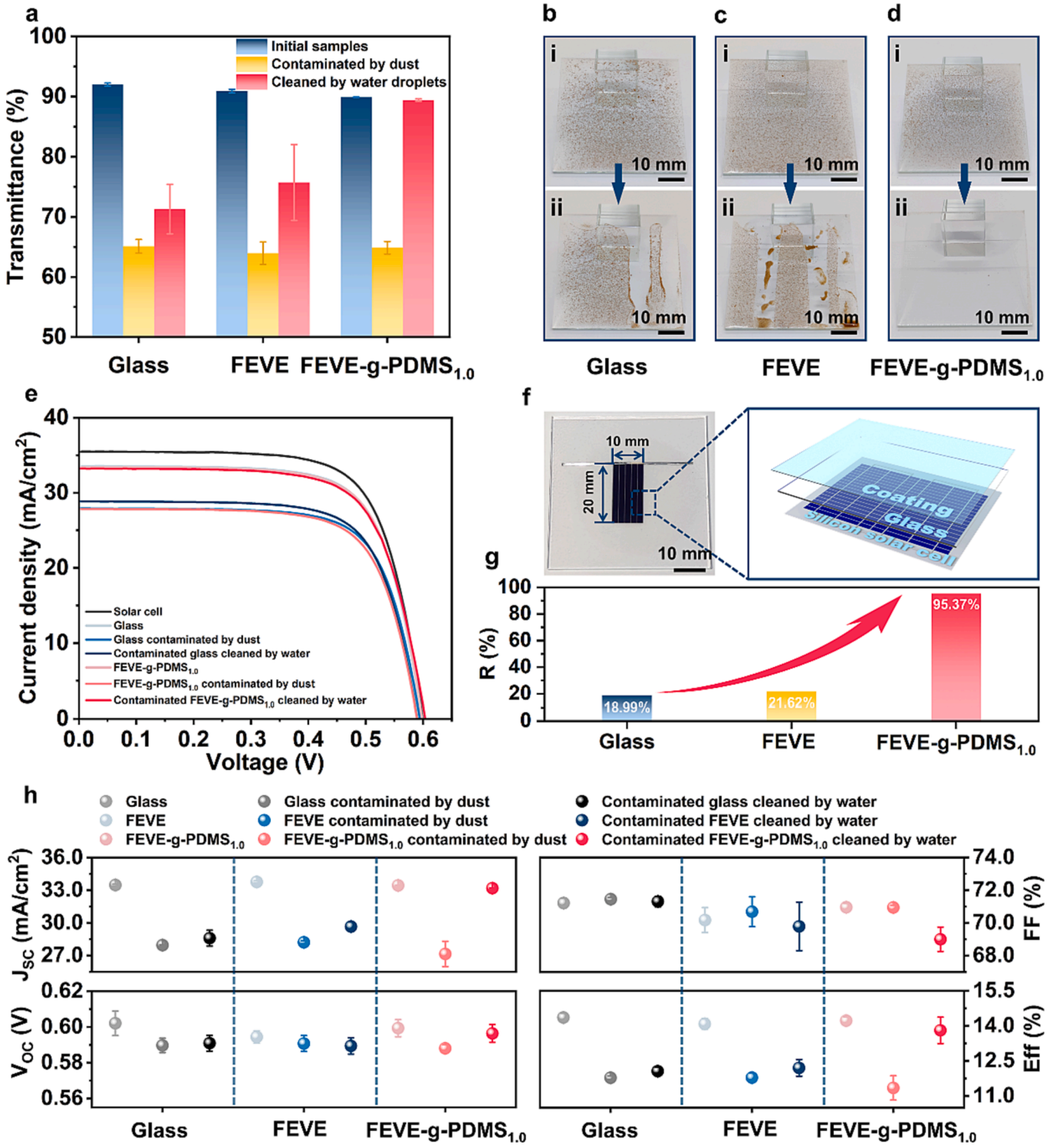

Fig. 6. (a) The visible light average transmittance of initial, contaminated, and cleaned samples (glass, FEVE coating, and FEVE-g-PDMS$_{1.0}$ coating). (b-d) Photographs of contaminated and cleaned samples ((b) glass, (c) glass coated with FEVE, (d) glass coated with FEVE-g-PDMS$_{1.0}$). (e) Comparison of *I-V* curves of the solar cells with different cover samples. (f) Photograph and schematic illustration of the solar cell used for *J-V* characteristic test. (g) The recovery ratio of different samples. (h) The J_{SC}, V_{OC}, *FF*, and *Eff* values of solar cells.

To deeply investigate the practicality of the omniphobic liquid-like FEVE-g-PDMS$_{1.0}$ coating in self-cleaning application for solar cells, the self-cleaning properties were quantified by measuring the current density–voltage (*J-V*) curves of the monocrystalline silicon solar cell covered with different coating samples under different conditions. As well known, the negative effects of dust and other stains on solar cells were most directly reflected in the loss of light transmittance. Obviously, the transmittance of bare glass, glass coated with FEVE coating and FEVE-g-PDMS$_{1.0}$ coating decreased to 63 ~ 65 % with D-value was 8 g/m^2 (Fig. 6a). After the self-cleaning process, the transmittance of FEVE coating only recovered to 75.71 %. In sharp contrast, the transmittance of cleaned FEVE-g-PDMS$_{1.0}$ coating was up to 89.42 %. Fig. 6b–d and Movie S1 substantiated that large areas of dust were still deposited on the surface of the glass and FEVE coating samples; however, the FEVE-g-PDMS$_{1.0}$ coating was as clean as before the dust deposition.

As demonstrated in Fig. 6e, the short-circuit current densities (J_{sc}) of a solar cell covered with bare glass (33.48 mA/cm^2) or glass coated with FEVE-g-PDMS$_{1.0}$ (33.44 mA/cm^2) had a slightly lower than a bare solar cell (35.50 mA/cm^2), because light passing through the glass or coated glass was inevitably lost compared to being exposed directly to the solar cell (photograph and schematic illustration in Fig. 6f shows the structure of the samples from top to bottom with the coating, glass, and solar cell). Nonetheless, J_{sc} of the solar cell covered with glass or coated glass were still quite similar, suggesting that the FEVE-g-PDMS$_{1.0}$ coating can be applied to the protective cover glass of solar cells without causing adverse effects. Moreover, once the contaminated sample with the same *D*-value was covered on the solar cell, whether it was glass or coated glass, the J_{sc} of the solar cell wolud be significantly reduced (27.82 ~ 28.21 mA/cm^2). Notably, after the self-cleaning operation was performed, the J_{sc} of the solar cell covered by FEVE-g-PDMS$_{1.0}$ coating recovered to 33.18 mA cm^{-2}, which was extremely close to that of the initial FEVE-g-PDMS$_{1.0}$ coating. Additionally, the ratio of recovered J_{sc} (R) was defined to evaluate the self-cleaning properties of the sample. As displayed in Fig. 6g, the R-values of the glass and FEVE coating samples were only 18.99 % and 21.62 %, respectively. By contrast, the FEVE-g-PDMS$_{1.0}$ coating with excellent self-cleaning properties showed an incredibly high R-value of 95.37 %. The results indicate that after the self-cleaning process, the J_{sc} of the solar cell was correspondingly significantly close to that before being contaminated by dust. Besides, based on *J-V* curves, the J_{SC}, V_{OC}, *FF*, and *Eff* values were summarized in Fig. 6h and Table S4. Taken together, these results indicate that FEVE-g-PDMS$_{1.0}$ coating with excellent self-cleaning property and high transparency can be applied to solar cells to efficiently remove deposited dust, thereby increasing the power conversion efficiency, extending the longevity, and reducing the operational and maintenance cost of solar cells.

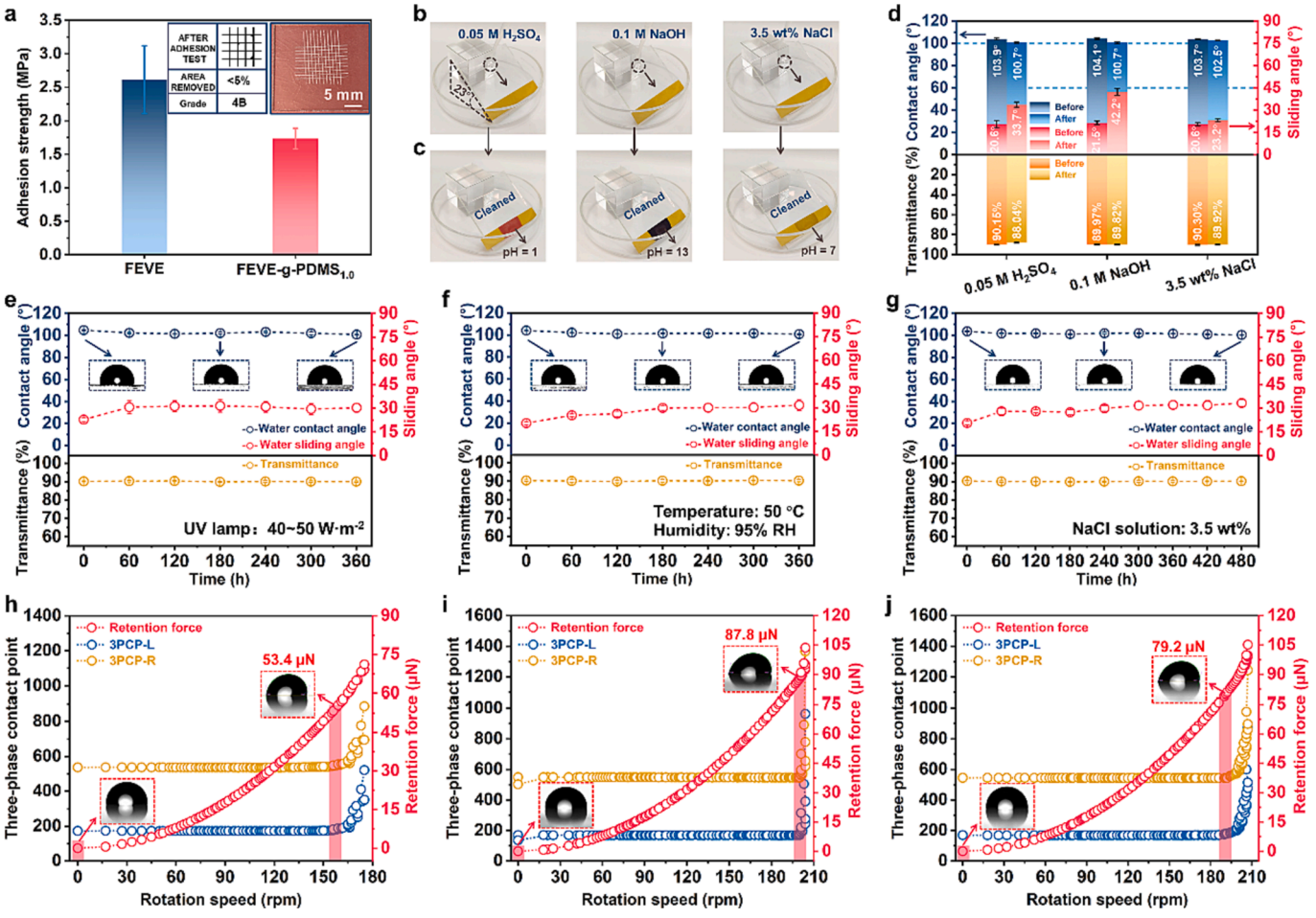

Fig. 7. (a) The adhesion strength test of FEVE and FEVE-g-PDMS$_{1.0}$ coating. Insets: The adhesion grade of cross-cut method test and photographs of FEVE-g-PDMS$_{1.0}$ coating after test. (b, c) Snapshots taken when sliding the H_2SO_4, NaOH, and NaCl droplets on the FEVE-g-PDMS$_{1.0}$ coating. (d) The WCA, WSA, and visible light average transmittance of the FEVE-g-PDMS$_{1.0}$ coating after immersing in H_2SO_4, NaOH, and NaCl solution for 12 h. (e) The variations of WCA, WSA and visible light average transmittance on the FEVE-g-PDMS$_{1.0}$ coating with an exposure time of UV lamp. (f, g) The variations of WCA, WSA, and visible light average transmittance on the FEVE-g-PDMS$_{1.0}$ coating with (f) exposure time in constant temperature humidity chamber and (g) immersion time in NaCl solution. (h-j) The curves of the three-phase contact point (3PCP) of both two ends of the water droplet and retention force as a function of rotation speed on FEVE-g-PDMS$_{1.0}$ coating after (h) UV-resistance, (i) humidity resistance and thermal stability, and (j) chemical durability tests.

3.4. Durability of the coatings

3.4.1. Adhesion strength, wear-resistance, and applicability

The adhesion strength of the coatings was tested quantificationally by cross-cut method and pull-off methods (Text S3). As displayed in Fig. 7a, the adhesion strength between the FEVE-g-PDMS$_{1.0}$ coating and the tempered float glass substrate reached 1.73 MPa. Moreover, after repeated peeling with high adhesive tape, the coating area loss was less than 5 %, indicating that the adhesion rating was 4B. The strong adhesion strength of the FEVE-g-PDMS$_{1.0}$ coating can be attributed to the following reasons: the interlocking effect between the cross-linked FEVE macromolecule network structure and the slightly rough float glass surface; the chemical reaction between the –NCO groups of cross-linking agent HDIT and the –OH groups on the glass surface; and the hydrogen bonding effect between –OH/–COOH groups of the FEVE matrix and –OH groups on the glass surface [52]. Moreover, the wear-resistance of the coating was also investigated, and the results showed that after 200 wear cycles, the coating remained highly transparent (visible light average transmittance = 89.77 %) and omniphobicity (WSA = 35.0°, OSA = 9.0°), with water droplets and oil droplets sliding off the coating surface easily (Text. S4 and Fig. S7).

Owing to the strong adhesion strength of the coatings and the facile spraying method, they can be coated on various substrates besides glass, such as carbon steel, tinplate, aluminum, PET film, and cotton fabric, and also displayed liquid-repellency, indicating the FEVE-g-PDMS$_{1.0}$ coating possesses high practical applicability (Fig. S8). Moreover, FEVE-g-PDMS$_{1.0}$ coating coatings could also be applied to larger substrates to satisfy practical requirements (Fig. S9).

3.4.2. Uv-resistance property

The polymer material used as a self-cleaning coating for protective solar cover glass admittedly has aging problems, where UV rays play a significant role in the structural damage of the material. So, the UV exposure test (Text S5) was performed to investigate the UV-resistance property of the FEVE-g-PDMS$_{1.0}$ coating. As shown in Fig. 7e, with the extension of UV exposure time, although the WSA of the coating increased slightly, it was still lower than 32°. Furthermore, after 360 h, the WCA and visible light average transmittance of the coating were consistently higher than 100.8° and 89.8 %, respectively, confirming that omniphobicity and transparency of the coating were not significantly negatively affected. The excellent UV-resistant property of the coating can be ascribed to the unique chemical inertness of FEVE resin and PDMS. On the one hand, the photon energy of UV rays was not sufficient to break the C-F bond with high bond disassociation energy in the fluoropolymer FEVE [21]. On the other hand, the rigid Si-O-Si bonds with high bond energy in PDMS were also difficult to be broken by UV rays, and the inorganic components in PDMS could resist the aging and degradation of UV rays [53].

3.4.3. Humidity resistance and thermal stability

Due to the variety of application environments, the self-cleaning coatings for solar cells are generally challenged by high temperatures and humidity. Herein, the FEVE-g-PDMS$_{1.0}$ coating was placed in a constant temperature humidity chamber (Text S6) to verify its humidity resistance and thermal stability. As can be seen in Fig. 7f, the FEVE-g-PDMS$_{1.0}$ coating maintained high WCA, low WSA, and high visible light average transmittance (100.8°, 31.6°, and 89.97 %, respectively) when the test time was extended to 360 h. Moreover, the appearance of the coating was retained well, and there were no blistering and peeling phenomena. These results were not only likely to be related to the excellent adhesion strength of the coating, but also to the 'discrete liquid–liquid interface' formed between the enriched PDMS chains on the coating surface and immiscible water/high moisture vapor, resulting in the liquid molecules were unlikely to permeate the coating [32].

3.4.4. Chemical durability

To further investigate the chemical durability of the FEVE-g-PDMS$_{1.0}$ coating (Text S7), the H_2SO_4 (pH = 1), NaOH (pH = 13), and NaCl (pH = 7) droplets were dropped onto the coating. Obviously, all droplets readily slide down the tilted coating, without leaving any trace behind (Fig. 7b, c and Movie S2). Additionally, as shown in Fig. 7d, the FEVE-g-PDMS$_{1.0}$ coatings were immersed in the above three solutions for 12 h, the WCA, visible light average transmittance, and WSA of the coating after immersing were higher than 100.7° and 88.04 %, and less than 42.2°, respectively. Moreover, Fig. 7g displayed the outstanding salt-water penetration resistance of the coating, which maintained WCA and WSA at 100.5° and 33.2° even after 480 h of immersion in neutral salt water, and with negligible loss of transmittance. These results indicated that the FEVE-g-PDMS$_{1.0}$ coating has high stability in various media and has the potential to satisfy the needs of the chemical durability required by solar cells. Moreover, the UV–vis transmission spectra of the above three coatings were shown in Fig. S10, confirming that the transmittance of the coatings is virtually unchanged throughout the visible spectral region. Furthermore, the coating prepared in this work showed relatively comprehensive properties by comparing them with those reported in the literature, which facilitates their practical application (Table S5).

Additionally, the retention forces between the FEVE-g-PDMS$_{1.0}$ coatings after UV-resistance, humidity resistance and thermal stability, and chemical durability tests and the water droplets were measured. Driven by centrifugal force, water droplet placed on the coating surface has a tendency to slide laterally, which causes the shape of the droplets to change. The retention force between the droplet and the surface is defined as the force corresponding to when the three-phase contact points (3PCP) at both the left and right ends of the droplet begin to deviate from their original positions. For the FEVE-g-PDMS$_{1.0}$ coating before tests, the retention force was 43.6 μN (Fig. S11). As shown in Fig. 7h–j, after the above three tests, the retention force of water droplets on the coatings were 53.4, 87.8, and 79.2 μN, respectively. moreover, the water droplets slid off the FEVE-g-PDMS$_{1.0}$ coating (after durability test) surface without residue, whereas water droplets on the FEVE coating stubbornly stayed on the surface at the same rotational speed. These results indicate the FEVE-g-PDMS$_{1.0}$ coating has excellent stability, especially the resistance to UV radiation, which is indispensable for the practical application of the coating.

3.5. Dynamic de-wetting and self-cleaning mechanisms

Based on all of the results that we have, the main dynamic de-wetting and self-cleaning mechanisms of omniphobic liquid-like FEVE-g-PDMS$_{1.0}$ coating were proposed and illustrated in Fig. 8. Fig. 8a and b illustrate the cross-linking structure and low sliding angle of FEVE-g-PDMS$_{1.0}$ coating, which shows the dynamic repellency towards liquids. Concretely, the dynamic de-wetting and self-cleaning mechanisms can be attributed to four aspects: (1) the smoothness and chemical homogeneity of the coating reduce the topographical and chemical defects on its surface, which is conducive to reducing the number of metastable states and energy barriers between them [54,55]; (2) the well-crosslinked coating network including FEVE matrix and embedded PDMS chains has abundant low-surface-energy groups (-CF_3, –CH_3), which enhance the permeability resistance and dynamic de-wetting property of the coating to the various probe liquids; (3) owing to the extremely low glass transition temperature of PDMS, the unbound and repeated (-O-Si-O-) groups in PDMS chains are liquid and highly flexible, and they can enrich on the coating surface and rotate/bend dynamically to exhibit liquid-like properties at room temperature, which endows the FEVE-g-PDMS$_{1.0}$ coating with the ability to overcome the energy barriers for moving the liquids [56,57]. (4) Based on the self-similarity of the structure and composition of the thick coating, the dynamic de-wetting property can be maintained after mechanical or chemical damage [33]. Besides, as shown in Fig. 8c and d, the PDMS chains embedded on coating surface can also be graphically illustrated by an

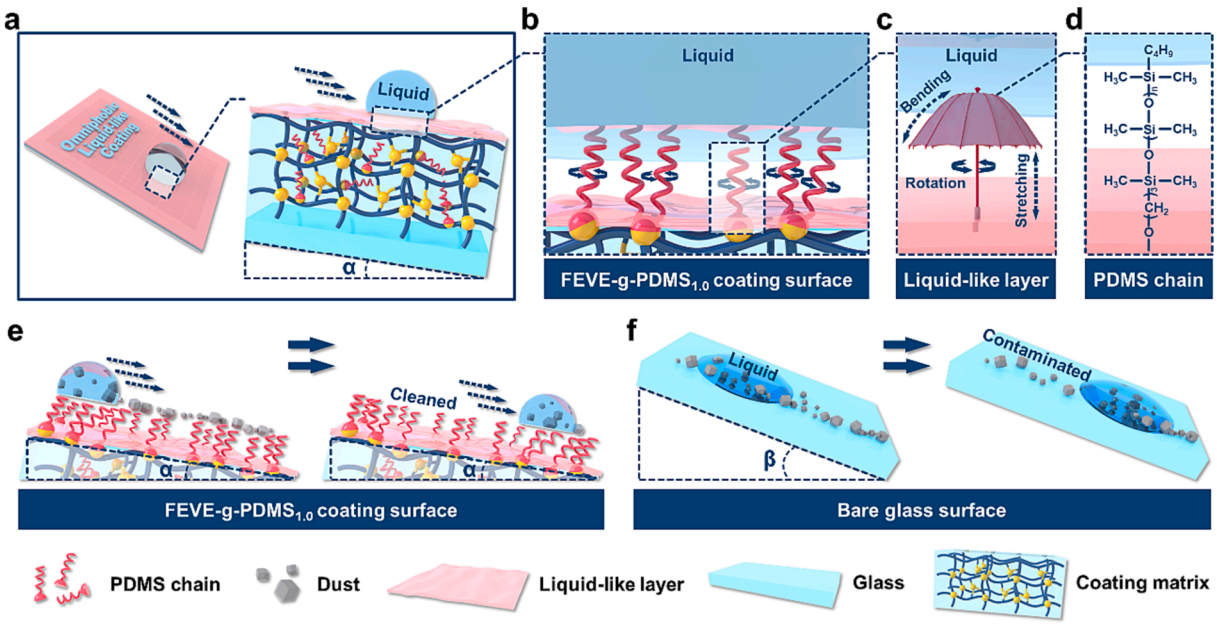

Fig. 8. (a–d) Schematic illustration of dynamic de-wetting mechanism of omniphobic liquid-like FEVE-g-PDMS$_{1.0}$ coating ((a, b) A schematic illustrating the crosslinking structure, low sliding angle, and liquid-repellency of the liquid-like coating surface, and the high mobility of PDMS chains, (c) 'Umbrella model' of high mobility of PDMS chains, (d) A schematic illustrating the molecular structure of PDMS chains). (e, f) Schematic illustration of self-cleaning mechanism ((e) omniphobic liquid-like FEVE-g-PDMS$_{1.0}$ coating, (f) bare glass). Schematics are not to scale and do not depict the precise molecular conformation of PDMS chains.

'umbrella model', i.e., the molecular chains exhibit efficient dynamic de-wetting property through continuous rotation and other movements [58,59].

As illustrated in Fig. 8e, the dust particles deposited on the coating surface can be successfully removed when the liquid droplets slide smoothly; however, even though the higher tilt angle has been applied, dust still stubbornly contaminates the bare glass surface (Fig. 8f). In conclusion, the FEVE-g-PDMS$_{1.0}$ coating with excellent dynamic de-wetting property and durability can be an appropriate candidate for self-cleaning application for solar cells and other optical devices.

4. Conclusion

In summary, we have created a highly transparent, durable, omniphobic liquid-like FEVE-g-PDMS$_{1.0}$ coating specifically designed to mitigate the dust deposition on solar cell glasses and aimed to enhance the efficiency for solar cells. The FEVE-g-PDMS$_{1.0}$ coating could be applied onto PV glass by facile spraying method, and the coating could exhibit high transparency with transmittance of 96.93 % at 550 nm. Moreover, by employing PDMS as low-surface-energy and flexible chains, the prepared coating showed liquid-like property and excellent omniphobicity/dynamic de-wetting behavior for various probe liquids and could maintain free-contaminated by allowing liquids to slip readily at low sliding angles. Such a dynamic de-wetting behavior endowed the FEVE-g-PDMS$_{1.0}$ coating with self-cleaning property, by effectively removing the deposited dust without leaving dust and water residue. In this case, the resultant coating demonstrated high efficiency recovery ratio for solar cells (95.37 %) with the consumption of cleaning water equivalent to a slight shower in nature. Furthermore, the obtained coating displayed good durability, including strong adhesion, UV-resistance, humidity and thermal stability, and could withstand the erosion of acid, alkali, and saline solutions. Therefore, it is believed that the omniphobic liquid-like FEVE-g-PDMS$_{1.0}$ coating in this work provided a new strategy for developing durable self-cleaning coating for solar cells, and is expected to be applied in many practical optical fields.

Declaration of Competing Interest

The authors declare that they have no known competing financial interests or personal relationships that could have appeared to influence the work reported in this paper.

Data availability

Data will be made available on request.

Acknowledgements

The research is financially supported by the National Key R&D Program of China (2022YFB3808800), the National Science Foundation for Distinguished Young Scholars of China (Grant No.51925403), the National Science Foundation of China (21676052, 21606042), and Tianjin Research Innovation Project for Postgraduate Students (2022BKY060).

Appendix A. Supplementary data

Supplementary data to this article can be found online at https://doi.org/10.1016/j.cej.2023.147090.

References

[1] F. Wang, J.D. Harindintwali, Z. Yuan, M. Wang, F. Wang, S. Li, Z. Yin, L. Huang, Y. Fu, L. Li, S.X. Chang, L. Zhang, J. Rinklebe, Z. Yuan, Q. Zhu, L. Xiang, D.C. W. Tsang, L. Xu, X. Jiang, J. Liu, N. Wei, M. Kastner, Y. Zou, Y.S. Ok, J. Shen, D. Peng, W. Zhang, D. Barcelo, Y. Zhou, Z. Bai, B. Li, B. Zhang, K. Wei, H. Cao, Z. Tan, L.B. Zhao, X. He, J. Zheng, N. Bolan, X. Liu, C. Huang, S. Dietmann, M. Luo, N. Sun, J. Gong, Y. Gong, F. Brahushi, T. Zhang, C. Xiao, X. Li, W. Chen, N. Jiao, J. Lehmann, Y.G. Zhu, H. Jin, A. Schaffer, J.M. Tiedje, J.M. Chen, Technologies and perspectives for achieving carbon neutrality, Innovation (camb) 2 (4) (2021), 100180, https://doi.org/10.1016/j.xinn.2021.100180.

[2] O. Ellabban, H. Abu-Rub, F. Blaabjerg, Renewable energy resources: Current status, future prospects and their enabling technology, Renew. Sustain. Energy Rev. 39 (2014) 748–764, https://doi.org/10.1016/j.rser.2014.07.113.

[3] N. Kannan, D. Vakeesan, Solar energy for future world: - a review, Renewable Sustainable Energy Rev. 62 (2016) 1092–1105, https://doi.org/10.1016/j.rser.2016.05.022.

[4] Ş. Kılkış, G. Krajačić, N. Duić, M.A. Rosen, M.d.A. Al-Nimr, Advances in integration of energy, water and environment systems towards climate neutrality for sustainable development, Energy Conver. Manage. 225 (2020), https://doi.org/10.1016/j.enconman.2020.113410.

[5] N. Cherupurakal, M.S. Mozumder, A.-H.-I. Mourad, S. Lalwani, Recent advances in superhydrophobic polymers for antireflective self-cleaning solar panels, Renew. Sustain. Energy Rev. 151 (2021), https://doi.org/10.1016/j.rser.2021.111538.

[6] C. Agustín-Sáenz, M. Machado, J. Nohava, N. Yurrita, A. Sanz, M. Brizuela, O. Zubillaga, A. Tercjak, Mechanical properties and field performance of hydrophobic antireflective sol-gel coatings on the cover glass of photovoltaic modules, Sol. Energy Mater. Sol. Cells 216 (2020), https://doi.org/10.1016/j.solmat.2020.110694.

[7] A.S. Sarkın, N. Ekren, Ş. Sağlam, A review of anti-reflection and self-cleaning coatings on photovoltaic panels, Sol. Energy 199 (2020) 63–73, https://doi.org/10.1016/j.solener.2020.01.084.

[8] N. Ababacar, M.K. Cheikh, A.N. Pape, C. Abderafi, K. Abdessamad, S. Vincent, Impact of dust on the photovoltaic (PV) modules characteristics after an exposition year in Sahelian environment: the case of senegal, Int. J. Phys. Sci. 8 (21) (2013) 1166–1173.

[9] S.C.S. Costa, A.S.A.C. Diniz, L.L. Kazmerski, Dust and soiling issues and impacts relating to solar energy systems: literature review update for 2012–2015, Renew. Sustain. Energy Rev. 63 (2016) 33–61, https://doi.org/10.1016/j.rser.2016.04.059.

[10] M.K. Smith, C.C. Wamser, K.E. James, S. Moody, D.J. Sailor, T.N. Rosenstiel, Effects of natural and manual cleaning on photovoltaic output, J. Sol. Energy Eng. 135 (3) (2013), https://doi.org/10.1115/1.4023927.

[11] A. Sayyah, M.N. Horenstein, M.K. Mazumder, Energy yield loss caused by dust deposition on photovoltaic panels, Sol. Energy 107 (2014) 576–604, https://doi.org/10.1016/j.solener.2014.05.030.

[12] M.R. Maghami, H. Hizam, C. Gomes, M.A. Radzi, M.I. Rezadad, S. Hajighorbani, Power loss due to soiling on solar panel: a review, Renew. Sustain. Energy Rev. 59 (2016) 1307–1316, https://doi.org/10.1016/j.rser.2016.01.044.

[13] M. Mazumder, M.N. Horenstein, J.W. Stark, P. Girouard, R. Sumner, B. Henderson, O. Sadder, I. Hidetaka, A.S. Biris, R. Sharma, Characterization of electrodynamic screen performance for dust removal from solar panels and solar hydrogen generators, IEEE Trans. Ind. Appl. 49 (4) (2013) 1793–1800, https://doi.org/10.1109/TIA.2013.2258391.

[14] A. Gheitasi, A. Almaliky, N. Albaqawi, Development of an automatic cleaning system for photovoltaic plants, IEEE PES Asia-Pacific Power and Energy Engineering Conference (APPEEC) 2015 (2015) 1–4.

[15] T. Sarver, A. Al-Qaraghuli, L.L. Kazmerski, A comprehensive review of the impact of dust on the use of solar energy: History, investigations, results, literature, and mitigation approaches, Renew. Sustain. Energy Rev. 22 (2013) 698–733, https://doi.org/10.1016/j.rser.2012.12.065.

[16] V. Gupta, M. Sharma, R.K. Pachauri, K.N. Dinesh Babu, Comprehensive review on effect of dust on solar photovoltaic system and mitigation techniques, Sol. Energy 191 (2019) 596–622, https://doi.org/10.1016/j.solener.2019.08.079.

[17] S.A.M. Said, G. Hassan, H.M. Walwil, N. Al-Aqeeli, The effect of environmental factors and dust accumulation on photovoltaic modules and dust-accumulation mitigation strategies, Renew. Sustain. Energy Rev. 82 (2018) 743–760, https://doi.org/10.1016/j.rser.2017.09.042.

[18] Q. Xu, Q. Zhao, X. Zhu, L. Cheng, S. Bai, Z. Wang, L. Meng, Y. Qin, A new kind of transparent and self-cleaning film for solar cells, Nanoscale 8 (41) (2016) 17747–17751, https://doi.org/10.1039/c6nr03537j.

[19] H. Zhong, Y. Hu, Y. Wang, H. Yang, TiO2/silane coupling agent composed of two layers structure: a super-hydrophilic self-cleaning coating applied in PV panels, Appl. Energy 204 (2017) 932–938, https://doi.org/10.1016/j.apenergy.2017.04.057.

[20] A. Syafiq, A.K. Pandey, N.N. Adzman, N.A. Rahim, Advances in approaches and methods for self-cleaning of solar photovoltaic panels, Sol. Energy 162 (2018) 597–619, https://doi.org/10.1016/j.solener.2017.12.023.

[21] A. Roslizar, S. Dottermusch, F. Vüllers, M.N. Kavalenka, M. Guttmann, M. Schneider, U.W. Paetzold, H. Hölscher, B.S. Richards, E. Klampaftis, Self-cleaning performance of superhydrophobic hot-embossed fluoropolymer films for photovoltaic modules, Sol. Energy Mater. Sol. Cells 189 (2019) 188–196, https://doi.org/10.1016/j.solmat.2018.09.017.

[22] Y. Liu, Q. Xu, A.M. Lyons, Durable, optically transparent, superhydrophobic polymer films, Appl. Surf. Sci. 470 (2019) 187–195, https://doi.org/10.1016/j.apsusc.2018.11.113.

[23] J.-J. Park, D.-Y. Kim, J.-G. Lee, D. Kim, J.-H. Oh, T.-Y. Seong, M.F.A.M. van Hest, S. S. Yoon, D. Johnson, Superhydrophilic transparent titania films by supersonic aerosol deposition, J. Am. Ceram. Soc. 96 (5) (2013) 1596–1601, https://doi.org/10.1111/jace.12164.

[24] P. Wang, X. Yan, J. Zeng, C. Luo, C. Wang, Anti-Reflective superhydrophobic coatings with excellent durable and Self-cleaning properties for solar cells, Appl. Surf. Sci. 602 (2022), https://doi.org/10.1016/j.apsusc.2022.154408.

[25] K. Chen, S. Zhou, S. Yang, L. Wu, Fabrication of all-water-based self-repairing superhydrophobic coatings based on uv-responsive microcapsules, Adv. Funct. Mater. 25 (7) (2014) 1035–1041, https://doi.org/10.1002/adfm.201403496.

[26] K. Chen, S. Zhou, L. Wu, Facile fabrication of self-repairing superhydrophobic coatings, Chem. Commun. 50 (80) (2014) 11891–11894, https://doi.org/10.1039/c3cc49251f.

[27] P. Liu, H. Zhang, W. He, H. Li, J. Jiang, M. Liu, H. Sun, M. He, J. Cui, L. Jiang, X. Yao, Development of "Liquid-like" copolymer nanocoatings for reactive oil-repellent surface, ACS Nano 11 (2) (2017) 2248–2256, https://doi.org/10.1021/acsnano.7b00046.

[28] W. Zheng, J. Huang, X. Zang, X. Xu, W. Cai, Z. Lin, Y. Lai, Judicious design and rapid manufacturing of a flexible, mechanically resistant liquid-like coating with strong bonding and antifouling abilities, Adv. Mater. 34 (42) (2022) 2204581, https://doi.org/10.1002/adma.202204581.

[29] Z. Ma, Y. Liu, K. Feng, J. Wei, J. Liu, Y. Wu, X. Pei, B. Yu, M. Cai, F. Zhou, Brush-like" amphiphilic polymer for environmental adaptive coating, ACS Appl Mater Interfaces 14 (16) (2022) 18901–18909, https://doi.org/10.1021/acsami.2c01824.

[30] X. Hao, Z. Sun, S. Wu, T.W. Wang, Y. Liu, Y. Wu, X. He, Q. Liu, F. Zhou, Self-lubricative organic-inorganic hybrid coating with anti-icing and anti-waxing performances by grafting liquid-like polydimethylsiloxane, advanced materials, Interfaces 9 (18) (2022), https://doi.org/10.1002/admi.202200160.

[31] Y. Liu, C. Qin, R. Xu, Y. Liu, Y. Wu, B. Yu, X. Pei, F. Zhou, Organic-inorganic hybrid polysiloxane brushes with improved lubrication and load-bearing capacity, Langmuir 38 (9) (2022) 2832–2839, https://doi.org/10.1021/acs.langmuir.1c02937.

[32] D.F. Cheng, C. Urata, M. Yagihashi, A. Hozumi, A statically oleophilic but dynamically oleophobic smooth nonperfluorinated surface, Angew. Chem. Int. Ed. 51 (12) (2012) 2956–2959, https://doi.org/10.1002/anie.201108800.

[33] M. Rabnawaz, G. Liu, H. Hu, Fluorine-free anti-smudge polyurethane coatings, Angew. Chem. Int. Ed. 54 (43) (2015) 12722–12727, https://doi.org/10.1002/anie.201504892.

[34] W. Pan, Q. Wang, J. Ma, W. Xu, J. Sun, X. Liu, J. Song, Solid-like slippery coating with highly comprehensive performance, Adv. Funct. Mater. 33 (31) (2023), https://doi.org/10.1002/adfm.202302311.

[35] X. Zhong, H. Hu, L. Yang, J. Sheng, H. Fu, Robust hyperbranched polyester-based anti-smudge coatings for self-cleaning, anti-graffiti, and chemical shielding, ACS Appl Mater Interfaces 11 (15) (2019) 14305–14312, https://doi.org/10.1021/acsami.8b22447.

[36] H. Lei, J. Xiao, L. Zheng, M. Xiong, Y. Zhu, J. Qian, Q. Zhuang, Z. Han, Superhydrophobic coatings based on colloid silica and fluorocopolymer, Polymer 86 (2016) 22–31, https://doi.org/10.1016/j.polymer.2016.01.026.

[37] P. Wang, M. Kong, W. Du, L. Wang, L. Ni, The effect of pollutants on leakage current and power degradation of photovoltaic modules, Renew. Energy 146 (2020) 2668–2675, https://doi.org/10.1016/j.renene.2019.08.055.

[38] P. Gao, Y. Wang, H. Wang, J. Wang, X. Men, Z. Zhang, Y. Lu, Liquid-like transparent and flexible coatings for anti-graffiti applications, Prog. Org. Coat. 161 (2021), https://doi.org/10.1016/j.porgcoat.2021.106476.

[39] X. Li, F. Bian, J. Hu, S. Li, X. Gui, S. Lin, One-step synthesis of novel multifunctional silicone acrylate prepolymers for use in UV-curable coatings, Prog. Org. Coat. 163 (2022), https://doi.org/10.1016/j.porgcoat.2021.106601.

[40] H. Sun, X. Liu, B. Yu, Z. Feng, N. Ning, G.-H. Hu, M. Tian, L. Zhang, Simultaneously improved dielectric and mechanical properties of silicone elastomer by designing a dual crosslinking network, Polym. Chem. 10 (5) (2019) 633–645, https://doi.org/10.1039/c8py01763h.

[41] P. Gao, Y. Wang, J. Wang, F. Wang, W. Ma, Z. Zhang, X. Men, Y. Lu, Rational design of durable anti-fouling coatings with high transparency, hardness, and flexibility, ACS Appl Mater Interfaces 14 (25) (2022) 29156–29166, https://doi.org/10.1021/acsami.2c04279.

[42] D. Wei, J. Zeng, Q. Yong, High-performance bio-based polyurethane antismudge coatings using castor oil-based hyperbranched polyol as superior cross-linkers, ACS Appl. Polym. Mater. 3 (7) (2021) 3612–3622, https://doi.org/10.1021/acsapm.1c00503.

[43] Z. Ha, L. Lei, M. Zhou, Y. Xia, X. Chen, P. Mao, B. Fan, S. Shi, Bio-based waterborne polyurethane coatings with high transparency, antismudge and anticorrosive properties, ACS Appl Mater Interfaces 15 (5) (2023) 7427–7441, https://doi.org/10.1021/acsami.2c21525.

[44] B. Lin, S. Zhou, Light-responsive nanoparticles with wettability changing from hydrophobicity to hydrophilicity and their application towards highly hydrophilic fluorocarbon coatings, Appl. Surf. Sci. 359 (2015) 380–387, https://doi.org/10.1016/j.apsusc.2015.10.111.

[45] H. Zhang, H. Liu, T. Chen, B. Wang, L. Zhou, C. Du, Fabrication of a fast curing super-hydrophobic FEVE/MMA coating and its property research, Mater. Sci. Eng. B 263 (2021), https://doi.org/10.1016/j.mseb.2020.114746.

[46] F. Wang, R. Chang, R. Ma, H. Qiu, Y. Tian, Eco-friendly and ph-responsive nano-starch-based superhydrophobic coatings for liquid-food residue reduction and freshness monitoring, ACS Sustain. Chem. Eng. 9 (30) (2021) 10142–10153, https://doi.org/10.1021/acssuschemeng.1c02090.

[47] D.K. Owens, R.C. Wendt, Estimation of the surface free energy of polymers, J. Appl. Polym. Sci. 13 (8) (1969) 1741–1747, https://doi.org/10.1002/app.1969.070130815.

[48] D.H. Kaelble, Dispersion-polar surface tension properties of organic solids, J. Adhes. 2 (2) (1970) 66–81, https://doi.org/10.1080/0021846708544582.

[49] D.F. Cheng, C. Urata, B. Masheder, A. Hozumi, A physical approach to specifically improve the mobility of alkane liquid drops, J. Am. Chem. Soc. 134 (24) (2012) 10191–10199, https://doi.org/10.1021/ja302903e.

[50] K. Chen, B. Zhao, S. Dai, G. Wang, J. Cui, D. Zhao, K. Yu, H. Qiu, Facile fabrication of transparent slippery coatings with dual self-healing ability, Appl. Surf. Sci. 639 (2023), https://doi.org/10.1016/j.apsusc.2023.158207.

[51] Z. Ma, Y. Wu, R. Xu, Y. Liu, Z. Li, J. Liu, X. Pei, W. Bu, F. Zhou, Brush-like organic-inorganic hybrid polysiloxane surface with omniphobicity and extreme durability, Prog. Org. Coat. 154 (2021), https://doi.org/10.1016/j.porgcoat.2021.106171.

[52] R. Yuan, H. Liu, Y. Chen, Z. Liu, Z. Li, J. Wang, G. Jing, Y. Zhu, P. Yu, H. Wang, Design ambient-curable superhydrophobic/electroactive coating toward durable pitting corrosion resistance, Chem. Eng. J. 374 (2019) 840–851, https://doi.org/10.1016/j.cej.2019.05.209.

[53] U. Eduok, O. Faye, J. Szpunar, Recent developments and applications of protective silicone coatings: A review of PDMS functional materials, Prog. Org. Coat. 111 (2017) 124–163, https://doi.org/10.1016/j.porgcoat.2017.05.012.
[54] L. Chen, S. Huang, R.H.A. Ras, X. Tian, Omniphobic liquid-like surfaces, Nat. Rev. Chem. (2023), https://doi.org/10.1038/s41570-022-00455-w.
[55] R. Lhermerout, H. Perrin, E. Rolley, B. Andreotti, K. Davitt, A moving contact line as a rheometer for nanometric interfacial layers, Nat. Commun. 7 (2016) 12545, https://doi.org/10.1038/ncomms12545.
[56] P.J. Rossky, Exploring nanoscale hydrophobic hydration, Faraday Discuss. 146 (2010) 13-8; discussion 79-101, 395-401. https://doi.org/10.1039/c005270c.
[57] W. Chen, A.Y. Fadeev, M.C. Hsieh, D. Öner, J. Youngblood, T.J. McCarthy, Ultrahydrophobic and ultralyophobic surfaces: some comments and examples, Langmuir 15 (10) (1999) 3395–3399, https://doi.org/10.1021/la990074s.
[58] L. Gao, T.J. McCarthy, Contact angle hysteresis explained, Langmuir 22 (14) (2006) 6234–6237, https://doi.org/10.1021/la060254j.
[59] A. Hozumi, T.J. McCarthy, ultralyophobic oxidized aluminum surfaces exhibiting negligible contact angle hysteresis, Langmuir 26 (4) (2010) 2567–2573, https://doi.org/10.1021/la9028518.